

## **Impedance Analysis of Magnesium Doped Hematite Thin Films**

\*Aseya Akbar<sup>1)</sup>, Saira Riaz<sup>2)</sup>, Shahid Atiq<sup>3)</sup>, Javaid Iqbal<sup>4)</sup>  
and Shahzad Naseem<sup>5)</sup>

<sup>1), 2), 3), 4), 5)</sup> *Centre of Excellence in Solid State Physics, University of the Punjab, Lahore, Pakistan*

<sup>5)</sup> [shahzad.cssp@pu.edu.pk](mailto:shahzad.cssp@pu.edu.pk)

### **ABSTRACT**

Iron oxide thin films have gained significant interest as material that offers impending applications in nano- and micro-devices. Hematite ( $\alpha\text{-Fe}_2\text{O}_3$ ) thin films can be utilized in solar cells, gas sensors and as tunnel barrier in spintronic devices. Structural and dielectric properties of hematite can be greatly enhanced with addition of dopant. For this purpose, un-doped and magnesium doped iron oxide thin films have been prepared using sol-gel and spin coating method. Dopant concentration is varied as 2%, 4% and 6%. XRD results confirm the formation of phase pure hematite at low temperature of 300°C. Shift of peak positions and changes in crystallite size and lattice parameters indicate that dopant has successfully replaced iron in the host lattice. Crystallite size increases as dopant concentration is increased to 4%. Further increase in dopant concentration results in lowering of crystallite size due to increased dislocations and strain. Impedance analyzer is used to study impedance and dielectric behavior of magnesium doped hematite thin films. Dielectric constant shows anomalous dispersion behavior i.e. increases at high frequencies. Tangent loss decreases as frequency of the field increases and becomes constant at high frequencies. Increase in crystallite size at dopant concentrations 2% and 4% results in decrease in internal stress that is favorable for the formation of 180° domains thus resulting in increased dielectric constant and decreased tangent loss. Cole-Cole plots indicate increase in grain and grain boundary resistance with increase in dopant concentration.

### **1. INTRODUCTION**

Due to scarcity of fossil fuels, there is a need to explore sustainable energy resources along with different energy conversion techniques. Metal oxides play a crucial role in this regard as they can be employed for various technological and industrial applications including biosensors and optoelectronic devices. Among various metal oxides, hematite ( $\alpha\text{-Fe}_2\text{O}_3$ ) is of considerable interest due to its chemical and thermal stability (Chakraborty et al. 2016, Aragon et al. 2016).

$\alpha\text{-Fe}_2\text{O}_3$  crystallizes in rhombohedral structure. It is also known to have the hexagonal structure. Each iron cation is surrounded by oxygen octahedron.  $\alpha\text{-Fe}_2\text{O}_3$  is formed with stoichiometric metal oxygen ratio. At low temperatures (<1400K) oxygen

evaporation is negligible. At temperatures higher than 1400K due to oxygen evaporation phase transition to magnetite takes place (Craik 1975). Iron cations in  $\alpha$ -Fe<sub>2</sub>O<sub>3</sub> have antiparallel arrangement below 960K. Spins in same plane are aligned parallel to each other while spins in the neighboring planes are antiparallel to each other. However, due to spin-orbit coupling uncompensated magnetic moments arise in the sublattice that produces weak ferromagnetic behavior in  $\alpha$ -Fe<sub>2</sub>O<sub>3</sub>. When temperature is lowered below 260K the spins become completely parallel thus resulting in transition of weak ferromagnetic to antiferromagnetic state. This temperature is known as “Morin temperature” (Riaz et al. 2014a, Akbar et al. 2014a).

There is always a keen interest in dielectric properties of oxide thin films for their use in microelectronic devices including high-density recording devices. However, the electrical conductivity of  $\alpha$ -Fe<sub>2</sub>O<sub>3</sub> is known not to be good between the Morin temperature and Neel temperature without the presence of impurities. This poor conductivity arises due to small drift mobility of carriers. These carriers need to be thermally activated in order to hop between different sites. In addition the conductivity in hematite is anisotropic in nature (Craik 1975). Therefore, the study of dielectric properties and conductivity needs to be carried out in detail before utilization of  $\alpha$ -Fe<sub>2</sub>O<sub>3</sub> in microelectronic devices. Further, dielectric properties and conductivity of  $\alpha$ -Fe<sub>2</sub>O<sub>3</sub> can be tuned with the help of various dopants (Vanagas et al. 2015, Mohapatra et al. 2013, Kulkarni and Lokhande 2003, Zhou et al. 2015).

Mg-doped  $\alpha$ -Fe<sub>2</sub>O<sub>3</sub> thin films were prepared using sol-gel and spin coating method. Effect of dopant on structural, dielectric properties and conductivity has been studied in detail.

## 2. EXPERIMENTAL DETAILS

Mg doped iron oxide thin films were deposited through sol-gel and spin coating technique. Fe(NO<sub>3</sub>)<sub>3</sub>.9H<sub>2</sub>O was used as precursor. Ethylene glycol and deionized water were taken as solvents. Sol was prepared by dissolving Fe(NO<sub>3</sub>)<sub>3</sub>.9H<sub>2</sub>O in solvents and heating at 80°C. Detailed synthesis steps have been reported elsewhere (Riaz et al. 2014a, Akbar et al. 2014). For magnesium doping, magnesium nitrate was mixed in solvent and was added to the sol with Mg content as 2%, 6% and 10%.

Copper (Cu) substrates were used to prepare iron oxide thin films. 1cm×1cm substrates were etched with diluted hydrochloric acid. The substrates were washed using deionized water. For removing organic contaminations acetone and isopropyl alcohol were used (Asghar et al. 2006a,b). Delta 6RC spin coater was used for deposition of films. After coating, films were annealed at 300°C

Structural and phase analysis of iron oxide thin films was determined using Bruker D8 Advance X-ray diffractometer. Dielectric properties were studied using 6500B Precision Impedance Analyzer.

## 3. RESULTS AND DISCUSSION

Fig. 1(a-c) shows XRD plots for Mg doped iron oxide films with dopant concentrations 2%, 6% and 10%. Peaks were matched with JCPDS card no. 87-1165 thus confirming  $\alpha$ -Fe<sub>2</sub>O<sub>3</sub> phase formation. No diffraction peaks related to magnesium oxide were observed in any of the XRD patterns and hence the presence of residual magnesium oxide can be ruled out. In addition, lattice distortions arising due to

presence of vacancies can lead to shift in the peak positions depending upon the presence of compressive or tensile strain in films. Substitution of  $Mg^{2+}$  in  $\alpha-Fe_2O_3$  lattice results in strain relaxation along with expansion of crystallite size (Kumari et al. 2015). At low dopant concentration of 6% the crystallinity of Mg doped hematite thin films increased as indicated by increase in intensity of diffraction peak of (202) plane. This is due to the formation of new nucleation centers that result from decrease in nucleation energy barrier with increase in dopant concentration (Najim and Rozaiq 2013). However, at high dopant concentration of 10% peak intensity corresponding to plane (202) decreases which is ascribed to increase in saturation of the new nucleation centers (Najim and Rozaiq 2013).

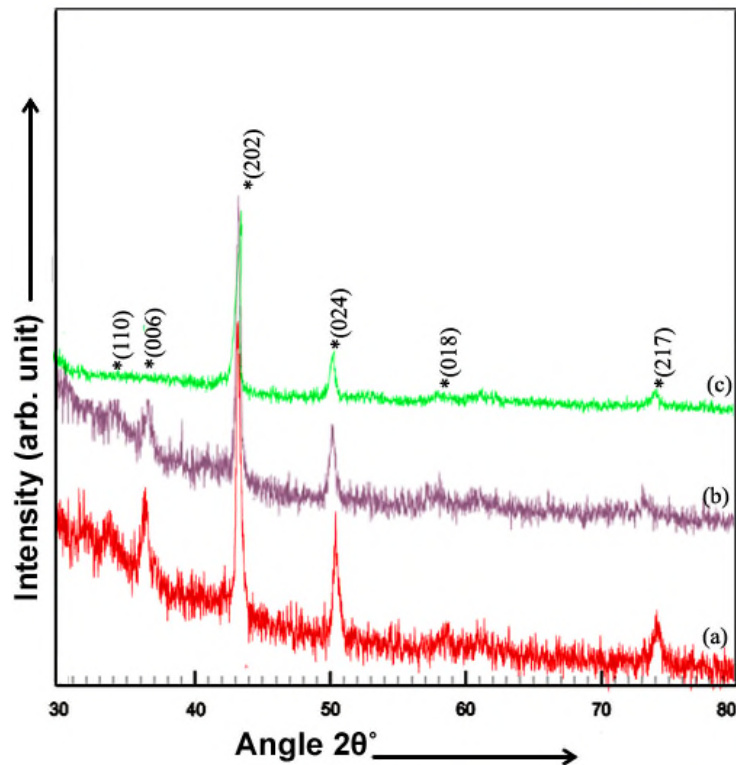


Fig. 1 XRD pattern for Mg doped hematite thin films with dopant concentration (a) 2% (b) 6% and (c) 10%

Crystallite size ( $t$ ), strain (Cullity 1956) and dislocation density ( $\delta$ ) (Kumar et al. 2011) were calculated using Eqs. 1-3.

$$t = \frac{0.9\lambda}{B \cos \theta} \quad (1)$$

$$\delta = \frac{1}{t^2} \quad (2)$$

$$Strain = \frac{\Delta d}{d} = \frac{d_{exp} - d_{hkl}}{d_{hkl}} \quad (3)$$

Where,  $\theta$  is the diffraction angle,  $\lambda$  is the wavelength (1.5406Å) and  $B$  is Full Width at Half Maximum.  $d_{exp}$  is the d-spacing calculated using XRD patterns in Fig. 1 and  $d_{hkl}$  is the d-spacing taken from JCPDS card 87-1165. Crystallite size (Fig. 2(a)) increased as Mg concentration was raised from 2% to 6%. Increase in crystallite size is related to increase in number of  $Mg^{2+}$  ions. These ions exert a drag force on the grain boundary motion and thus leading to grain growth (Najim and Rozaiq 2013). At higher dopant concentration of 10% the Mg atoms residing on grain boundaries increases. This causes decrease in crystallite size and increase in strain (Fig. 2(b)).

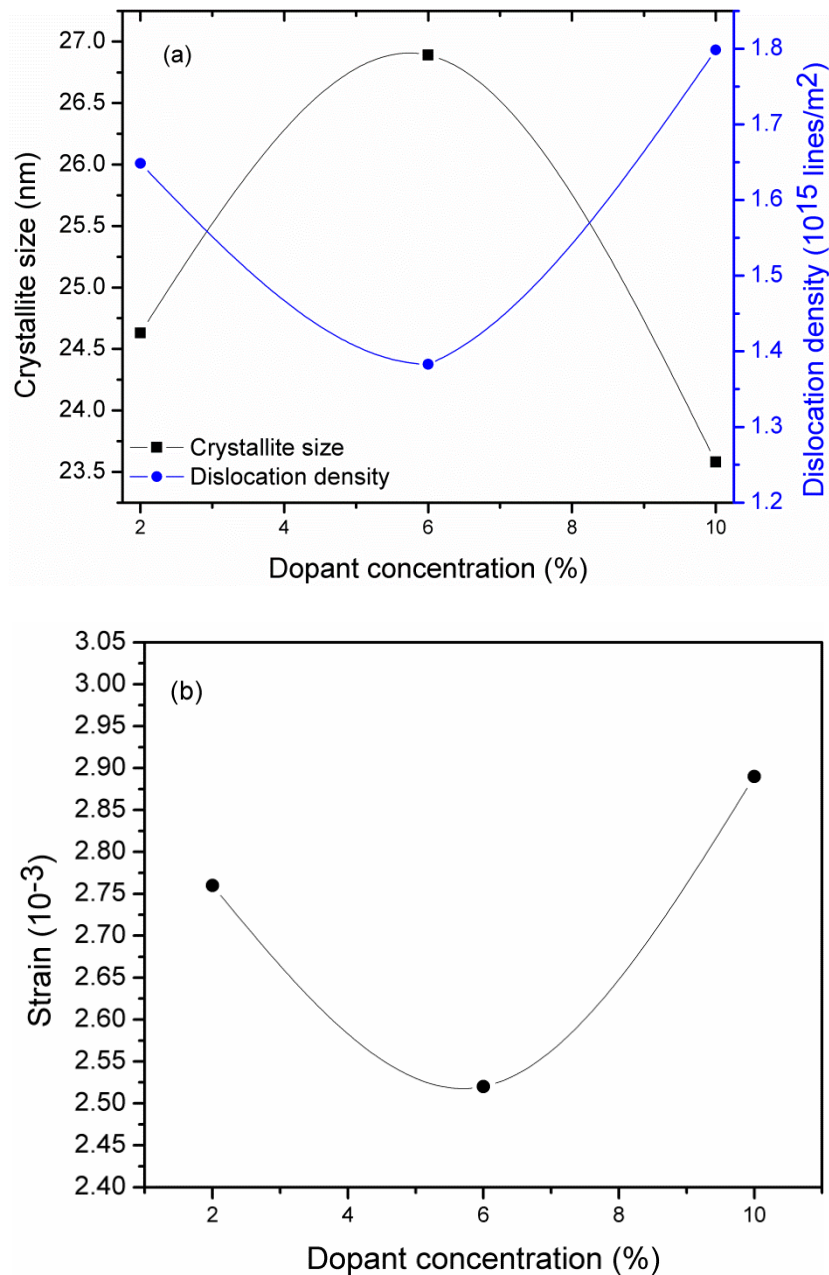


Fig. 2 (a) Crystallite size and dislocation density (b) Strain plotted as a function of dopant concentration

Lattice parameters ( $a$ ,  $c$ ) and x-ray density ( $\rho$ ,  $\text{g/cm}^3$ ) (Cullity 1956) were determined using Eqs. 4-5.

$$\sin^2 \theta = \frac{\lambda^2}{3a^2} (h^2 + k^2 + hk) + \frac{\lambda^2 l^2}{4c^2} \quad (4)$$

$$\rho = \frac{1.66042 \Sigma A}{V} \quad (5)$$

Where,  $\Sigma A$  is the sum of atomic weights of the atoms in the unit cell and  $V$  is the volume of unit cell in  $\text{\AA}^3$ .

Volume of unit cell (Table 1) increases with increase in Mg content. Increase in volume of unit cell is due to higher ionic radius of  $\text{Mg}^{2+}$  ( $0.72\text{\AA}$ ) as compared to  $\text{Fe}^{3+}$  ( $0.645\text{\AA}$ ) cations.

Table 1 shows lattice parameters, unit cell volume and X-ray density for Mg doped hematite thin films.

Dopant concentration (%)	Lattice parameters ( $\text{\AA}$ )		Unit cell volume ( $\text{\AA}^3$ )	X-ray density ( $\text{g/cm}^3$ )
	a	c		
2	5.02	13.630	297.4549	5.416792
6	5.024	13.656	298.4975	5.397874
10	5.029	13.678	299.5738	5.378481

Dielectric constant ( $\epsilon$ ) and tangent loss ( $\tan \delta$ ) were determined using Eqs. 6 and 7 (Barsoukov and Macdonald 2005).

$$\epsilon = \frac{Cd}{\epsilon_0 A} \quad (6)$$

$$\tan \delta = \frac{1}{2\pi f \epsilon_0 \epsilon \rho} \quad (7)$$

Where,  $C$  is the capacitance of films,  $d$  is the film thickness,  $\epsilon_0$  is the permittivity of free space,  $A$  is the area,  $f$  is the frequency and  $\rho$  is the resistivity. Dielectric constant (Fig. 3(a)) and tangent loss (Fig. 3(b)) decreased as frequency increased showing constant behavior at higher frequencies. Dispersion in these dielectric properties at low frequencies arises because of polarization of space charges and changes in valence state of cations present in the lattice. Frequency independent region at high frequencies arises because of the reason that electric dipoles are not able to follow the changes in externally applied electric field (Ghodake et al. 2016). Dispersion observed in the present case can be clarified by Maxwell–Wagner Model in accordance with Koop's phenomenological theory. According to Koop, a heterogeneous system is considered to be composed of two layers: 1) Conducting grains; 2) Highly resistive grain boundaries. The dielectric dispersion arises from interfacial polarization that

results from heterogeneity in the structure due to presence of grains and grain boundaries. Electrons hop through the conducting grains and pile up at grain boundaries. This results in increase in interfacial polarization and thus increased dielectric constant was observed (Riaz et al. 2015). In addition, electronic and ionic polarizations contribute to dielectric constant at low frequencies. At high frequencies only electronic polarization affects the dielectric constant. This results in high dielectric constant and low tangent loss at low frequencies while both of these factors were observed to decrease at high frequencies.

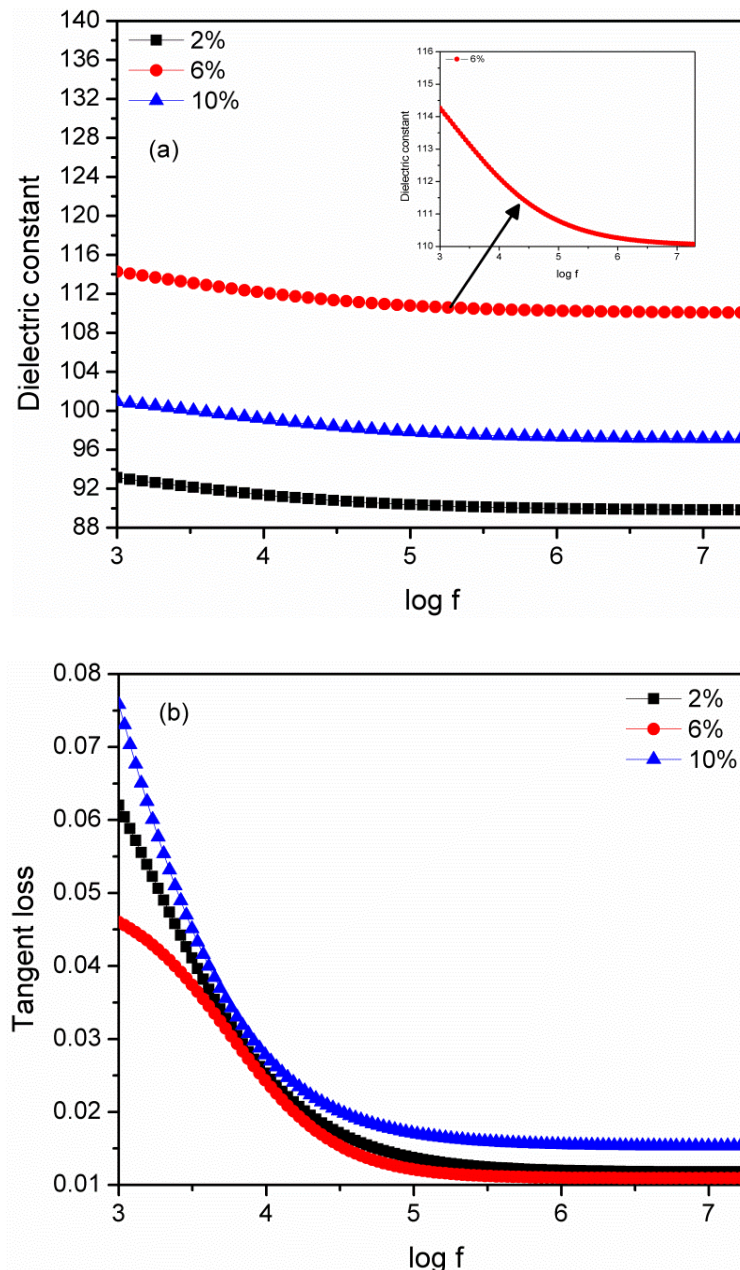


Fig. 3 (a) Dielectric constant (b) Tangent loss for Mg doped hematite thin films

Variation of dielectric constant and tangent loss by varying dopant concentration is shown in Fig. 4. Dielectric constant increased with increase in Mg concentration to 6%. At Mg concentration of 10% decrease in dielectric constant and increase in tangent loss was observed. Such phenomenon might have been observed because of the reason that at low dopant concentration ( $\leq 6\%$ ) domain walls of  $Mg^{2+}$  cations in host lattice moved easily. In addition, in order to maintain charge neutrality in hematite lattice  $Mg^{2+}$  cations replace  $Fe^{3+}$  cations thereby creating vacancies. These vacancies lead to reduction in strain, as observed in Fig. 2(b), therefore facilitating the domain wall motion and resulting in increase in dielectric properties (Sun et al. 2015). But, at high dopant concentration ( $>6\%$ ) dopant atoms segregated at grain boundaries and hence resulted in destruction of crystalline order and dielectric properties.

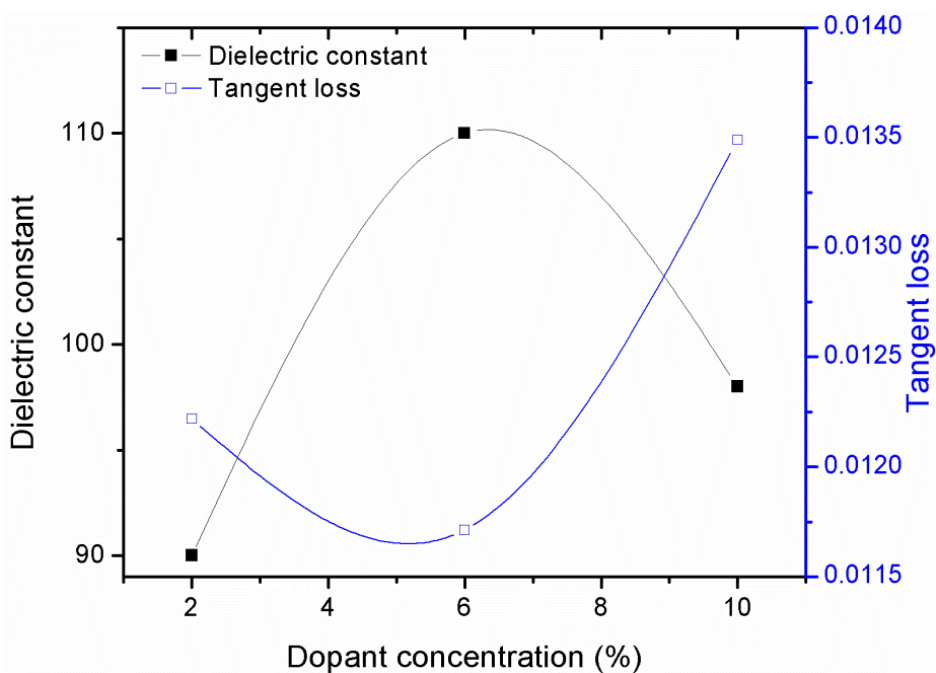


Fig. 4 Dielectric constant and tangent loss plotted as a function of dopant concentration

Conductivity ( $\sigma$ ) of these thin films was calculated using Eq. 8 (Barsoukov and Macdonald 2005).

$$\sigma = 2\pi f \epsilon \epsilon_0 \tan \delta \quad (8)$$

Conductivity of Mg doped hematite thin films can be seen in Fig. 5. Conductivity of hematite thin films remained constant in low frequency region ( $\log f = 5.0$ ) and is referred to as d.c. conduction. In high frequency region ( $\log f > 5.0$ ) conductivity of doped hematite thin films increased. D.C. conduction in dielectric material is based on free charge carriers that are mobile. On the other hand, a.c. conduction is because of the presence of bound charge carriers that hop from one potential well to another through tunneling process (Jamal et al. 2011). Increase in conductivity with increase in

Mg concentration depicts the applications of Mg doped  $\alpha\text{-Fe}_2\text{O}_3$  thin films as potential candidate for high density recording (Shinde et al. 2011).

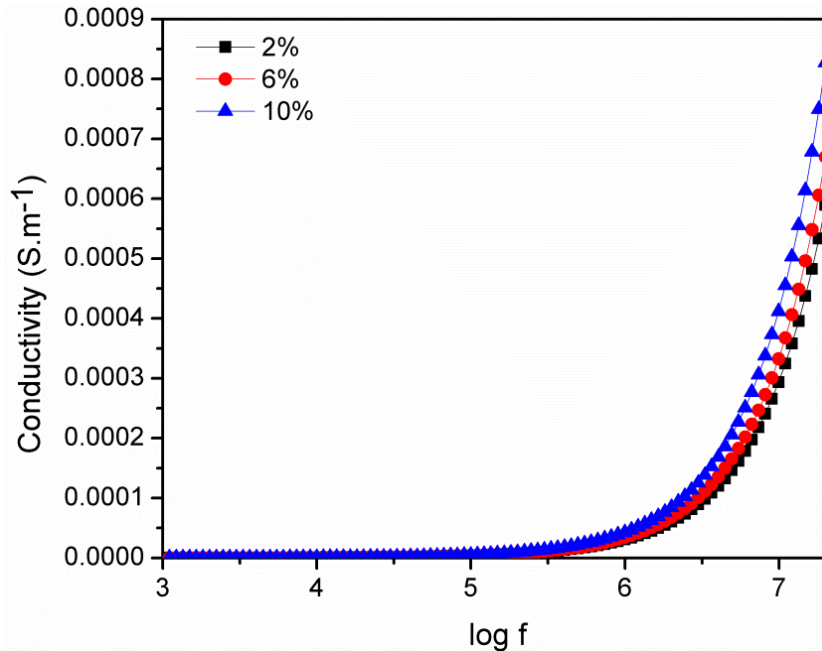


Fig. 5 Conductivity of Mg doped hematite thin films

Real impedance ( $Z'$ ) and Imaginary impedance ( $Z''$ ) are plotted as a function of  $\log f$  in Fig. 6. It can be seen in Fig. 6(a) that  $Z'$  remained constant at low frequencies and showed sharp decrease as frequency was increased. Furthermore,  $Z'$  became constant at high frequencies. On the other hand,  $Z''$  increased with increase in frequency and attained a maximum value and then decreased. This peak is attributed to the presence of resonance effect in Mg doped hematite thin films. Change in width and position of the relaxation peak is indicative that the relaxation process is affected by changes in dopant concentration (Barsoukov and Macdonald 2005).

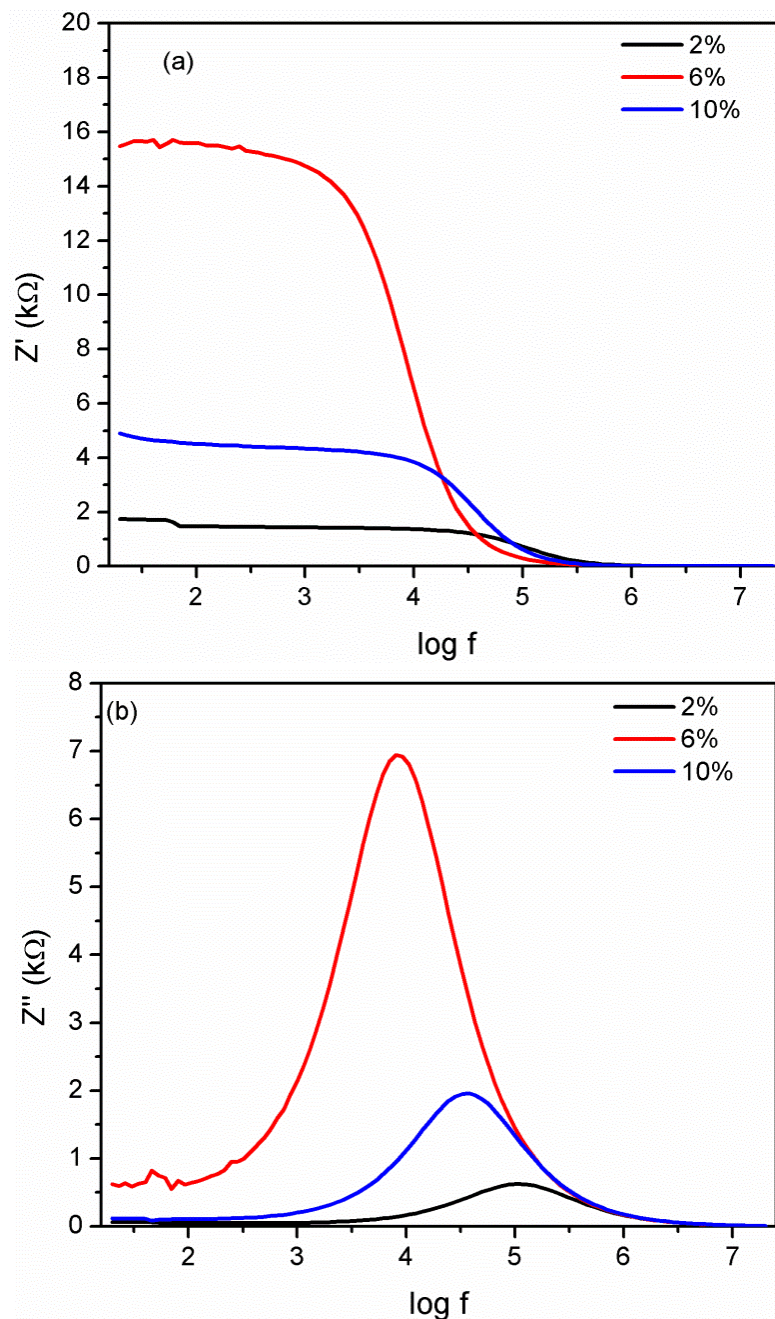


Fig. 6 (a) Real impedance (b) Imaginary impedance for Mg doped hematite thin films

#### 4. CONCLUSIONS

Magnesium doped hematite thin films were deposited using sol-gel spin coating technique. Mg content was varied as 2%, 6% and 10%. X-ray diffraction patterns indicated the formation of phase pure hematite under all dopant conditions. Increase in dopant concentration up to 6% resulted in increased crystallite size and dielectric constant values. High conductivity at high dopant concentration made these films potential candidate for high density recording. Relaxation process in Mg doped hematite thin films was strongly affected by dopant concentration indicated by changes

in real and imaginary impedance parts.

## REFERENCES

- Akbar, A. Riaz, S. Ashraf, R. and Naseem, S. (2014), "Magnetic and magnetization properties of Co-doped Fe<sub>2</sub>O<sub>3</sub> thin films", *IEEE Trans. Magn.*, **50**, 2201204.
- Aragon, F.F.H. Ardisson, J.D. Aquinoa, J.C.R. Gonzalez, I. Macedo, W.A.A. Coaquira, J.A.H. Mantilla, J. Silva, S.W. and Morais, P.C. (2016), "Effect of the thickness reduction on the structural, surface and magnetic properties of  $\alpha$ -Fe<sub>2</sub>O<sub>3</sub> thin films", *Thin Solid Films*, **607**, 50–54.
- Asghar, M.H. Placido, F. and Naseem, S. (2006(a)), "Characterization of reactively evaporated TiO<sub>2</sub> thin films as high and medium index layers for optical applications", *Eur. Phys. J. - Appl. Phys.*, **35**, 177-184.
- Asghar, M.H. Placido, F. and Naseem, S. (2006(b)), "Characterization of Ta<sub>2</sub>O<sub>5</sub> thin films prepared by reactive evaporation", *Eur. Phys. J. - Appl. Phys.*, **36**, 119-124.
- Barsoukov, E. and Macdonald, J.R. (2005), "Impedance Spectroscopy: Theory, Experiment, and Applications," John Wiley & Sons, Inc., New Jersey.
- Chakraborty, M. Ghosh, A. Thangavel, R. and Asokan, K. (2016), "Conduction mechanism in mesoporous hematite thin films using low temperature electrical measurements and theoretical electronic band structure calculations", *J. Alloys Compd.*, **664**, 682-689.
- Cullity, B.D. (1956), "Elements of x-ray diffraction," Addison Wesley Publishing Company, USA.
- Ghodake, U.R. Chaudhari, N.D. Kambale, R.C Patil, J.Y. and Suryavanshi, S.S. (2016), "Effect of Mn<sup>2+</sup> substitution on structural, magnetic, electric and dielectric properties of Mg–Zn ferrites", *J. Magn. Magn. Mater.*, **407**, 60–68.
- Glasscock, J.A. Barnes, P.R.F. Plumb, I.C. Bendavid, A. and Martin, P.J. (2008), "Structural, optical and electrical properties of undoped polycrystalline hematite thin films produced using filtered arc deposition", *Thin Solid Films*, **516**, 1716–1724.
- Jamal, E.M.A. Kumar, D.S. and Anantharaman, M.R. (2011), "On structural, optical and dielectric properties of zinc aluminate nanoparticles", *Bull. Mater. Sci.*, **34**, 251–259.
- Kulkarni, S.S. and Lokhande, C.D. (2003), "Structural, optical, electrical and dielectrical properties of electrosynthesized nanocrystalline iron oxide thin films", *Mater. Chem. Phys.*, **82**, 151–156.
- Kumari, R. Sahai, A. and Goswami, N. (2015), "Effect of nitrogen doping on structural and optical properties of ZnO nanoparticles", *Prog. Nat. Sci.: Mater. Int.*, **25**, 300–309.
- Mohapatra, M. Layek, S. Anand, S. Verma, H.C. and Mishra, B.K. (2013), "Structural and magnetic properties of Mg-doped nano- $\alpha$ -Fe<sub>2</sub>O<sub>3</sub> particles synthesized by surfactant mediation– precipitation technique", *Phys. Stat. Solidi B*, **250**, 65–72.
- Najim, J.A. and Rozaiq, J.M. (2013), "Effect Cd doping on the structural and optical properties of ZnO thin films", *Int. Lett. Chem. Phys. Astro.*, **15**, 137-150.
- Riaz, S. and Naseem, S. (2007), "Effect of reaction temperature and time on the structural properties of Cu(In,Ga)Se<sub>2</sub> thin films deposited by sequential elemental layer technique", *J. Mater. Sci. Technol.*, **23**, 499-503.

- Riaz, S. Akbar, A. and Naseem, S. (2014a), "Ferromagnetic effects in Cr-Doped Fe<sub>2</sub>O<sub>3</sub> thin films", *IEEE Trans. Magn.*, **50**, 2200704.
- Riaz, S. Shah, S.M.H. Akbar, A. Atiq, S. Naseem, S. (2015), "Effect of Mn doping on structural, dielectric and magnetic properties of BiFeO<sub>3</sub> thin films", *J. Sol-Gel Sci. Technol.*, **74**, 329-339.
- Shinde, S.S. Bhosale, C.H. and Rajpure, K.Y. (2011), "Studies on morphological and electrical properties of Al incorporated combusted iron oxide", *J. Alloy Compd.*, **509**, 3943–3951.
- Sun, H. Zhang, Y. Liu, X. Guo, S. Liu, Y. and Chen, W. (2015), "The effect of Mn/Nb doping on dielectric and ferroelectric properties of PZT thin films prepared by sol-gel process", *J. Sol-Gel Sci. Technol.*, **74**, 378–386.
- Vanags, M. Sutka, A. Kleperis, J. and Shipkovs, P. (2015), "Comparison of the electrochemical properties of hematite thin films prepared by spray pyrolysis and electrodeposition", *Ceram. Int.*, **41**, 9024–9029.
- Zhou, Z. Huo, P. Guo, L. and Prezhdo, O.V. (2015), "Understanding hematite doping with group IV elements: A DFT+U study", *J. Phys. Chem. C*, **119**, 26303–26310.